Multidimensional analyses of proinsulin peptide-specific regulatory T cells induced by tolerogenic dendritic cells

Suwandi, Jessica S.; Laban, Sandra; Vass, Kincső; Joosten, Antoinette; van Unen, Vincent; Lelieveldt, Boudewijn; Höllt, Thomas; Zwaginga, Jaap Jan; Nikolic, Tatjana; Roep, Bart O.

DOI
10.1016/j.jaut.2019.102361

Publication date
2019

Document Version
Final published version

Published in
Journal of Autoimmunity

Citation (APA)
Suwandi, J. S., Laban, S., Vass, K., Joosten, A., van Unen, V., Lelieveldt, B., Höllt, T., Zwaginga, J. J., Nikolic, T., & Roep, B. O. (2019). Multidimensional analyses of proinsulin peptide-specific regulatory T cells induced by tolerogenic dendritic cells. *Journal of Autoimmunity*, *107 (2020)*, 1-11. Article 102361. https://doi.org/10.1016/j.jaut.2019.102361

Journal of Autoimmunity 107 (2020) 102361

Contents lists available at ScienceDirect

Journal of Autoimmunity

journal homepage: www.elsevier.com/locate/jautimm

Multidimensional analyses of proinsulin peptide-specific regulatory T cells induced by tolerogenic dendritic cells

Jessica S. Suwandi[a,1], Sandra Laban[a,1], Kincső Vass[a], Antoinette Joosten[a], Vincent van Unen[a,2], Boudewijn P.F. Lelieveldt[b], Thomas Höllt[c,d], Jaap Jan Zwaginga[a,e], Tatjana Nikolic[a,1], Bart O. Roep[a,f,*,1]

[a] Department of Immunohematology and Blood Transfusion, Leiden University Medical Center, Leiden, Netherlands
[b] Department of LKEB Radiology, Leiden University Medical Center, Leiden, Netherlands
[c] Computational Biology Center, Leiden University Medical Center, Leiden, Netherlands
[d] Computer Graphics and Visualization, Delft University of Technology, Delft, Netherlands
[e] Sanquin Research, Center for Clinical Transfusion Research and Jon J van Rood Center for Clinical Transfusion Science, Leiden University Medical Center, Leiden, Netherlands
[f] Department of Diabetes Immunology, Diabetes & Metabolism Research Institute at the Beckman Research Institute, City of Hope, USA

ARTICLE INFO

Keywords:
Regulatory T cells
Tolerogenic dendritic cells
Immune therapy
Mass cytometry

ABSTRACT

Induction of antigen-specific regulatory T cells (Tregs) *in vivo* is the holy grail of current immune-regulating therapies in autoimmune diseases, such as type 1 diabetes. Tolerogenic dendritic cells (tolDCs) generated from monocytes by a combined treatment with vitamin D and dexamethasone (marked by $CD52^{hi}$ and $CD86^{lo}$ expression) induce antigen-specific Tregs. We evaluated the phenotypes of these Tregs using high-dimensional mass cytometry to identify a surface-based T cell signature of tolerogenic modulation. Naïve $CD4^+$ T cells were stimulated with tolDCs or mature inflammatory DCs pulsed with proinsulin peptide, after which the suppressive capacity, cytokine production and phenotype of stimulated T cells were analysed. TolDCs induced suppressive T cell lines that were dominated by a naïve phenotype ($CD45RA^+CCR7^+$). These naïve T cells, however, did not show suppressive capacity, but were arrested in their naïve status. T cell cultures stimulated by tolDC further contained memory-like ($CD45RA^-CCR7^-$) T cells expressing regulatory markers Lag-3, CD161 and ICOS. T cells expressing $CD25^{lo}$ or $CD25^{hi}$ were most prominent and suppressed $CD4^+$ proliferation, while $CD25^{hi}$ Tregs also effectively supressed effector $CD8^+$ T cells.

We conclude that tolDCs induce antigen-specific Tregs with various phenotypes. This extends our earlier findings pointing to a functionally diverse pool of antigen-induced and specific Tregs and provides the basis for immune-monitoring in clinical trials with tolDC.

1. Introduction

T regulatory cells (Tregs) are specialized to control auto-immune responses and therefore vital in maintaining immune homeostasis. In type 1 diabetes, however, loss of tolerance to β-cell antigens results in the destruction of insulin-producing cells. Strategies to induce or increase Tregs have been developed in an effort to reduce immune inflammation in patients with autoimmune diseases[1–5]. In an attempt to induce islet antigen-specific Tregs, we established that dendritic cells (DCs) treated with $1,25(OH)_2$ vitamin D3 (1,25-dihydroxycholecalciferol; VitD3) and dexamethasone (VitD3/Dex) during their modulation and maturation from monocytes induce antigen-specific Tregs *in vitro* [6–9]. These tolerogenic DCs (tolDC) additionally show various suitable functional traits such as islet autoantigen-dependent inhibition of effector T cells [6], elimination of cytotoxic $CD8^+$ T cells [10,11] and homing characteristics to the disease lesion [8,12]. Moreover, the effect of tolDC was demonstrated *in vivo* using a humanized transgenic mouse model, where proinsulin peptide-pulsed tolDCs

* Corresponding author. Department of Immunohematology and Blood Transfusion, Leiden University Medical Center, Leiden, Netherlands.
E-mail addresses: j.s.suwandi@lumc.nl (J.S. Suwandi), s.laban@lumc.nl (S. Laban), a.m.joosten@lumc.nl (A. Joosten), v.van_unen@lumc.nl (V. van Unen), b.p.f.lelieveldt@lumc.nl (B.P.F. Lelieveldt), t.hoellt@lumc.nl (T. Höllt), j.j.zwaginga@lumc.nl (J.J. Zwaginga), t.nikolic@lumc.nl (T. Nikolic), broep@coh.org (B.O. Roep).
[1] These authors contributed equally to this work.
[2] Current address: Institute for Immunity, Transplantation and Infection, Stanford University School of Medicine, Stanford, USA.

https://doi.org/10.1016/j.jaut.2019.102361
Received 5 June 2019; Received in revised form 6 November 2019; Accepted 6 November 2019
Available online 24 November 2019

prevented and reversed autoimmunity to proinsulin[13]. Therapy with tolDCs loaded with specific antigens therefore appears a promising approach to reduce autoimmunity and introduce antigen-specific tolerance in type 1 diabetes. The safety of this strategy has been tested recently in a phase I clinical trial (https://www.trialregister.nl/trial/5425).

One of the major challenges encountered in immunomodulating trials is the lack of specific surface markers to determine the induction of adaptive immune tolerance, including induction or expansion of adaptive Tregs *in vivo*. Naturally occurring Tregs (nTregs) show consistent expression of the intracellular transcription factor Foxp3 that is often used as a Treg specification marker[14]. Although the role of Foxp3 as biomarker of tolerance is evident[15,16], both adaptive Tregs, e.g. Tr1 cells [17,18], show low or transient expression of Foxp3 similar to activated effector T cells [19,20]. In contrast, other surface molecules such as Lag-3, CTLA-4, PD-1, ICOS, CCR4, CD39, HLA-DR are present on subsets of nTreg [21] as well as on adaptive Tregs [8,22] and may be more useful for detection of induced suppressive T cells. Moreover, our previous data on tolDC-induced Tregs pointed to a diversity of Treg subtypes at a clonal level based on the intracellular cytokines and suppressive mechanisms[22]. Further determining the cell surface maker signatures of tolDC-induced Tregs may provide means for monitoring Treg induction in human trials.

In this study, we applied mass cytometry (CyTOF) detecting 35 surface markers simultaneously. The innovative Cytosplore software [23] enabled analyses of this high-dimensional data set with single-cell resolution using Hierarchical Stochastic Neighbor Embedding (HSNE) [23–25]. This novel approach enabled us to extend previous studies with current in depth investigation of surface marker expression patterns of proinsulin-specific Tregs induced by tolDCs and to correlate to their capacity to suppress T cell proliferation.

2. Material and methods

2.1. Generation and quality control of human tolDCs and mDCs

Human peripheral blood mononuclear cells (PBMC) were isolated with Ficoll density gradient centrifugation from HLA-typed buffy coats purchased from Sanquin. All participants have given a written informed consent. The protocol of generating monocyte derived mDCs and tolDCs has been described[6]. After 48 h of activation with LPS (100 ng/mL) and human GM-CSF (800 U/mL), matured tolDCs and mDCs were stained for FACS analysis. Cells were washed with FACS buffer (PBS/0.5%BSA/0.02%Azide) and stained with APC-labelled PD-L1 (clone MIH1, Ebioscience, Cat# 17-5983-42, Lot# E12159-1634) and CD25 (clone M-A251, BD, Cat# 560987, Lot# 5176736), FITC-labelled CD52 (clone YTH34.5, Serotec AbD, Cat# MCA1642F, Lot# 0215) and PE-labelled CD86 (clone 2331, BD, Cat# 560957, Lot# 5128592). Flow cytometric staining was analysed on the FACS Canto II (BD) and data analysis was performed using FlowJo V10.

2.2. Inducing T_{tolDC} and T_{mDC} lines from naïve $CD4^+$ T cells

Cryopreserved immature tolDCs and control DCs were thawed and activated for 48 h with LPS (100 ng/mL, Sigma-Aldrich Chemie) in the presence of human GM-CSF (800 U/mL, Invitrogen). Naïve autologous $CD4^+$ T cells were isolated from CD14 negative fraction using untouched human $CD4^+$ T cell kit (Dynal, Invitrogen) or naïve $CD4^+$ T cell isolation kit (MACS, Miltenyi Biotec), according to the suppliers' protocol. To exclude the possibility that suppressive T cells expand or arise from activated nTregs, $CD25^{hi}$ T cells were depleted in the isolation method of naïve $CD4^+$ T cells. Activated tolDCs or mDCs were loaded with proinsulin peptide C19A3 for 4 h (7.5 μg/ml) and co-cultured with naïve $CD4^+$ T cells to induce antigen specific T cell lines (T_{tolDC} and T_{mDC} respectively) as described previously [9].

2.3. Flow cytometry based sorting of T cells

T_{tolDC} and T_{mDC} lines were activated for 24 h with mDCs pulsed with C19A3 peptide as previously described and stained for sorting. Staining was performed on ice. Cells were washed with PBS/2%FCS and stained with APC-Cy7-labelled CD25 (clone M-A251, BD, Cat# 557753, Lot# 64916) and AF700-labelled CD45RA (clone HI100, Biolegend, Cat# 555365, Lot# B227350) for 30 min. Thereafter, cells were washed twice and taken up in PBS/2%FCS. Finally, sorting was done on FACSAria III (BD) and cells were collected in 50% FCS and 50% IMDM.

2.4. Suppression of allogeneic naïve $CD4^+$ T cells

To assess capacity of T_{tolDC} and T_{mDC} lines to suppress proliferation of naïve $CD4^+$ T cells, allogeneic donors (donor A) were selected to mismatch with the DC and T cell donors (donor B) bearing HLA-DR4 (the HLA restriction element of the proinsulin peptide C19A3), to allow quantification of antigen-specific suppression. Naïve $CD4^+$ T cells from donor A were labelled with 0.5 μM/ml CFSE (per $2*10^6$ cells/ml) and cultured in the presence of activated and C19A3 loaded mDCs from donor B at a 10:1 ratio in a 96 round bottom plate, coated with 0.1 μg/ml anti-human CD3 mAb (clone UCHT1, BD). Purified naïve T cells (control for crowding), T_{tolDC} or T_{mDC} cells from donor B were added at a 1:1 ratio to the CFSE labelled responder T cells. Each condition was tested in triplicate. After 4 days, cells were recovered and analysed on the FACS Calibur (BD). Prior to the analysis, 10,000 Flow-Count Fluorospheres were added (Beckman Coulter). For each sample, 5000 fluorosphere events were acquired for quantitative comparison of samples. Division (d) of responder cells were calculated as expansion index (EI) using de formula (n = number of divisions):

$$\int_{d=0}^{d=n} EI\ (d) = \frac{\sum \text{Events}(d)}{\sum Events(d)/2^n}$$

An expansion index of 1.0 (no division) forms the 0% proliferation value. Proliferation of CFSE labelled naïve $CD4^+$ T cells in the presence of naïve $CD4^+$ T cells (crowding control) forms the 100% proliferation value.

2.5. Suppression of cytotoxic $CD8^+$ T cells

To assess whether T_{tolDC} and T_{mDC} lines suppress cytotoxic $CD8^+$ T cells, a cytotoxicity assay was performed using B cell line (JY) as target cells and clonal PPI-specific $CD8^+$ T cells as effector[10]. Target B cells were labelled with a high dose of CFSE (1 μM/ml), representing a bystander target ($CFSE^{high}$) or labelled with a low dose of CFSE (0.1 μM/ml) and pulsed PPI peptide (5 μg/ml) to serve as a specific target ($CFSE^{low+PPI}$) of PPI-specific $CD8^+$ T cells. $CFSE^{low+PPI}$ and $CFSE^{high}$ target cells were co-cultured overnight with sorted T_{tolDC} in 1:1:2 ratio. During the last 4 h, PPI-specific $CD8^+$ T cells were added in 1:1 and 1:5 (specific target: effector) ratio, after which cells were recovered and analysed on the FACS Calibur (BD). Each condition was tested in duplicate. Percentage killing was calculated by using the formula:

$$Lysis = L(x) = \frac{(a-b)}{a+b}$$

a = $CFSE^{high}$ target cell
b = $CFSE^{low+PPI}$ target cell

$$\%\ Inhibition = 100 - \frac{L(T_{tolDC}) - L(\text{no } CD8)}{L(no\ T_{tolDC}) - L(no\ CD8)} * 100\%$$

Specific lysis was calculated by normalizing for spontaneous cell death in the absence of PPI-specific $CD8^+$ T cells. Inhibition of specific lysis was calculated by dividing specific killing in the presence of a T_{tolDC} line or a sorted cell subset with specific killing with PPI-specific $CD8^+$ T cells added alone (100% lysis).

2.6. Intracellular Foxp3 staining

T_{tolDC} were stimulated overnight with C19A3-pulsed mDC and washed with FACS buffer. Cells were fixed and thereafter stained with AF647-labelled Foxp3 (clone 259D, Beckman Coulter, Cat# B30650) in permeabilizing reagent (PerFix-nc Kit, Beckman Coulter) for 1 h at room temperature. Fluorescent staining was measured on the FACS Calibur (BD).

2.7. Cytokine release assays

T_{tolDC} and T_{mDC} cells were stimulated for 24 h with activated mDCs loaded with C19A3 peptide at a 10:1 ratio in a 96 round bottom plate. Supernatant was taken and stored at −80 °C until analysis. Cytokine analysis was done with Luminex 9-plex kit of BioRad according to the manufacturer's protocol.

2.8. Staining T_{tolDC} and T_{mDC} lines for CyTOF and data acquisition

The CyTOF antibody staining panel consisted of 35 surface markers including markers described for Tregs, lineage, differentiation and activation (Table 1). Metal-conjugated antibodies were either purchased or conjugated as described previously[26]. T_{tolDC} and T_{mDC} lines were activated for 24 h with mDCs pulsed with C19A3 peptide and stained for CyTOF analysis. For this, cryopreserved T_{tolDC} and T_{mDC} lines were thawed, washed and stimulated overnight with C19A3 peptide loaded mDC at a 10:1 ratio in a 96 round bottom plate. Staining was performed the next day, as previously described[26].

Table 1
Staining panel for mass cytometry.

Marker	Metal	Clone	Dilution
CD3	170Er	UCHT1	1:100
CD4	145Nd	RPA-T4	1:200
CD7	153Eu	CD7-6B7	1:100
CD8a	146Nd	RPA-T8	1:50
CD16	148Nd	3G8	1:100
CD20[a]	163Dy	2H7	1:200
CD25	149Sm	2A3	1:100
CD27	167Er	O323	1:100
CD28[a]	171 Yb	CD28.2	1:100
CD38	172 Yb	HIT2	1:200
CD39[a]	162Dy	A1	1:100
CD45	89Y	HI30	1:100
CD45RA	169 Tm	HI100	1:100
CD45RO[a]	173 Yb	UCHL1	1:100
CD49b[a]	176 Yb	P1e6c5	1:100
CD69	144Nd	FN50	1:50
CD103[a]	155Gd	Ber-ACT8	1:50
CD107 (LAMP)[a]	143Nd	H4A3	1:50
CD122[a]	158Gd	TU27	1:50
CD126 (IL6R)[a]	154Sm	UV4	1:40
CD127	165Ho	AO19D5	1:200
CD152 (CTLA4)[a]	166Er	14D3	1:40
CD161	164Dy	HP-3G10	1:100
CD194 (CCR4)	156Gd	L291H4	1:100
CD196 (CCR6)	141Pr	G034E3	1:100
CD197 (CCR7)	159 Tb	G043H7	1:100
CD223 (Lag-3)	150Nd	874501	1:40
CD278 (ICOS)	151Eu	DX29	1:50
CD279 (PD-1)	175Lu	EH 12.2H7	1:100
CD335 (NKp46)[a]	174 Yb	9E2	1:50
CD336 (Nkp44)[a]	147Sm	P44-8	1:50
CD357 (GITR)[a]	142Nd	621	1:40
HLA-DR[a]	168Er	L243	1:200
KLRG-1[a]	160Gd	REA261	1:50
TCRgd	152Sm	11F2	1:50

[a] Self-conjugated.

2.9. Analysis of CyTOF data

Live and single cells were distinguished using DNA stains and event length in FlowJo V10. Beads were excluded and cells were gated to be $CD4^+$, $CD45^+$, $TCRgd^-$ and $CD8^-$, and used for further analysis. PCA analysis of samples was performed using Partek software, version 7.0 2018 (Partek Inc., St. Louis, MO, USA). Next, SPADE trees were generated in Cytobank[27] with 200 target number nodes and 10% down sampled event target. Finally, dimensionality reduction technique HSNE implemented in Cytosplore[25] (version 2.2.0) was used for in-depth analysis of the dataset without down sampling. The amount of hierarchical levels suitable for HSNE analysis was determined with the formula $\log_{10}$ (n/100) and was set to 4 (n = 1,016,321 cells). Values were Arcsine transformed and HSNE analysis was performed based on the expression of the 35 markers listed in Table 1. Using the Gaussian-mean-shift method subsequent clusters were generated. Heatmaps were generated using R software (R package, version 99.902). Packages 'flowcore', 'ggplot 2', 'gplots' and 'heatmap.2' were used to assist in clustering and heatmap drawing.

2.10. Statistics

Statistical analysis was performed with GraphPad Prism version 7.00 (GraphPad Software, La Jolla California, USA). To compare differences in suppression and fold-expansion between T_{tolDC} and T_{mDC} lines, data were compared by a two-sided Student's t-test (paired). One-way ANOVA followed by Dunnett's multiple comparisons test was used to compare the suppression of sorted T cell populations. Cytokine production of T_{tolDC} and T_{mDC} lines was compared using Wilcoxon matched-pairs signed-rank test, statistical significance was corrected for multiple comparisons with the Benjamini and Hochberg procedure. Median expression values were normalized by log 10 transformation and subsequently analysed using multiple t-tests, statistical significance was corrected for multiple comparisons using the Holm-Sidak method.

3. Results

3.1. TolDCs expressing low CD86 induce suppressive T cell lines

Naïve $CD4^+$ T cells were stimulated by proinsulin peptide C19A3-loaded autologous tolDC or matured inflammatory DCs (mDC) (the generated T cell cultures further referred to as T_{tolDC} and T_{mDC}, respectively). After two rounds of antigen-specific stimulation, T_{tolDC} and T_{mDC} cells were tested in a suppression assay using a previously established protocol[6,8,9,22,28]. In short, proliferation of allogeneic CFSE labelled naïve $CD4^+$ T cells in the presence of T_{tolDC} or T_{mDC} and C19A3-pulsed mDC (10:10:1 ratio T_{CFSE}: T_{tolDC}/T_{mDC}: DC) was measured after 4 days of co-culturing. The proliferation of CFSE-labelled responder T cells was suppressed in the presence of T_{tolDC} cells whereas enhanced in the presence of T_{mDC} cells, compared to the proliferation in the presence of purified naïve T cells as crowding control (paired *t*-test; p = 0.04; Fig. 1A). Two out of eight T_{tolDC} lines showed no suppressive activity (Fig. 1A), which was associated with the inability to induce tolDCs expressing low levels of CD86 (Fig. 1D). This is in line with our previous report where low CD86 expression was important to characterize tolerogenic modulation of DCs [6,29]. Indeed, other characteristics of these two non-suppressive T_{tolDC} lines were also discordant with suppressive $T_{tolDC.}$ In the suppressive T_{tolDC} lines, the yield was similar to the number of naïve T cells at the start of culture, whereas the cell number in the two non-suppressive T_{tolDC} lines increased 3 and 8 fold compared to the start (Fig. 1B). The yield of T cells stimulated by mDCs was on average 12-fold higher after culture (paired *t*-test; p = 0.003) (Fig. 1B). The production of IL-5, IL-10, IL-13, IFN-g and TNF-a was evaluated after re-stimulation with C19A3-pulsed mDCs. Suppressive T_{tolDC} lines produced significantly lower amounts of IL-5, IL-10, IL-13 and TNFa as compared to their T_{mDC} counterparts

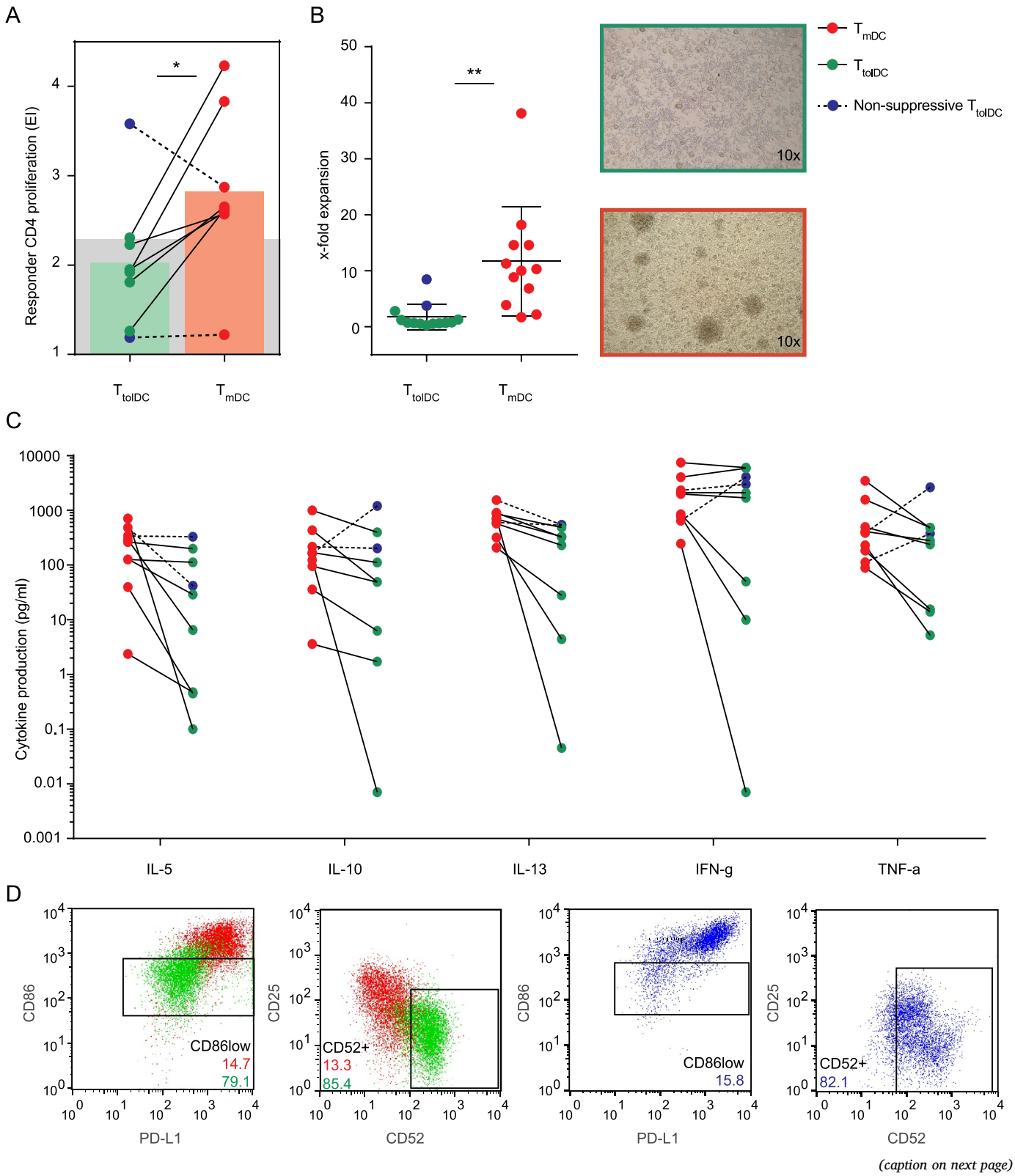

(caption on next page)

(Wilcoxon signed-rank test; p = 0.019 for all cytokines; Fig. 1C), whereas this trend was not observed in non-suppressive T_{tolDC} lines. Altogether, T cells stimulated with tolDCs or mDCs showed a dichotomy in suppressive capacity and cytokine production, while tolDCs expressing high CD86 induced non-suppressive T cells similar to mDC stimulated cultures.

3.2. High-dimensional phenotype analysis of T_{tolDC} and T_{mDC} lines with mass cytometry

To extensively characterize the surface phenotype of the suppressive T cells induced by tolDCs, we employed CyTOF technology to analyse five independently generated T_{tolDC} lines and corresponding T_{mDC} lines, of which one was a non-suppressive T_{tolDC} line. The median expression

Fig. 1. TolDC phenotype correlates with the capacity to induce suppressive T cells. A) The suppressive capacity of T_{tolDC} and T_{mDC}. mDCs pulsed with C19A3 were co-cultured with CFSE-labelled allogeneic naïve $CD4^+$ T cells in the presence of T_{tolDC} or T_{mDC} (ratio 1:10:10). Proliferation was calculated based on the expansion index (EI) and the grey bar depicts the proliferation in presence of naïve $CD4^+$ T cells (crowding control). T_{tolDC} inhibited the proliferation of naïve $CD4^+$ T cells, whereas T_{mDC} stimulated the proliferation of naïve $CD4^+$ T cells, n = 8 per group (paired *t*-test; p = 0.045). Two T_{tolDC} lines (blue symbols) did not suppress proliferation of responder $CD4^+$ T cells, compared to the autologous T_{mDC} line. **B)** Fold expansion of T cells in culture. T cells stimulated with mDC expanded on average 12-fold, whereas tolDC -stimulated T cells did not increase in number after two weeks co-culture, n = 12 per group (paired *t*-test p = 0.003). The two non-suppressive T_{tolDC} lines did expand 3-fold and 8- fold in culture. Picture inserts show T cells after 5 days of co-culture with tolDC (green frame) or mDC (red frame). **C)** Cytokine production by T_{tolDC} and T_{mDC} during overnight stimulation with proinsulin peptide-pulsed mDC. T_{mDC} lines produced significantly more IL-5, IL-10, IL-13 and TNF-a than suppressive T_{tolDC} lines, n = 7 per group (Wilcoxon signed rank test; p = 0.019 for all four cytokines). Non-suppressive T_{tolDC} were not included in the statistical analysis. **D)** Left panel shows representative phenotype of tolDCs (green) and mDCs (red) used to stimulate T cells determined by CD86 and CD52 expression. Right panel shows the phenotype of tolDCs used to induce the non-suppressive T_{tolDC} line (blue). (For interpretation of the references to colour in this figure legend, the reader is referred to the Web version of this article.)

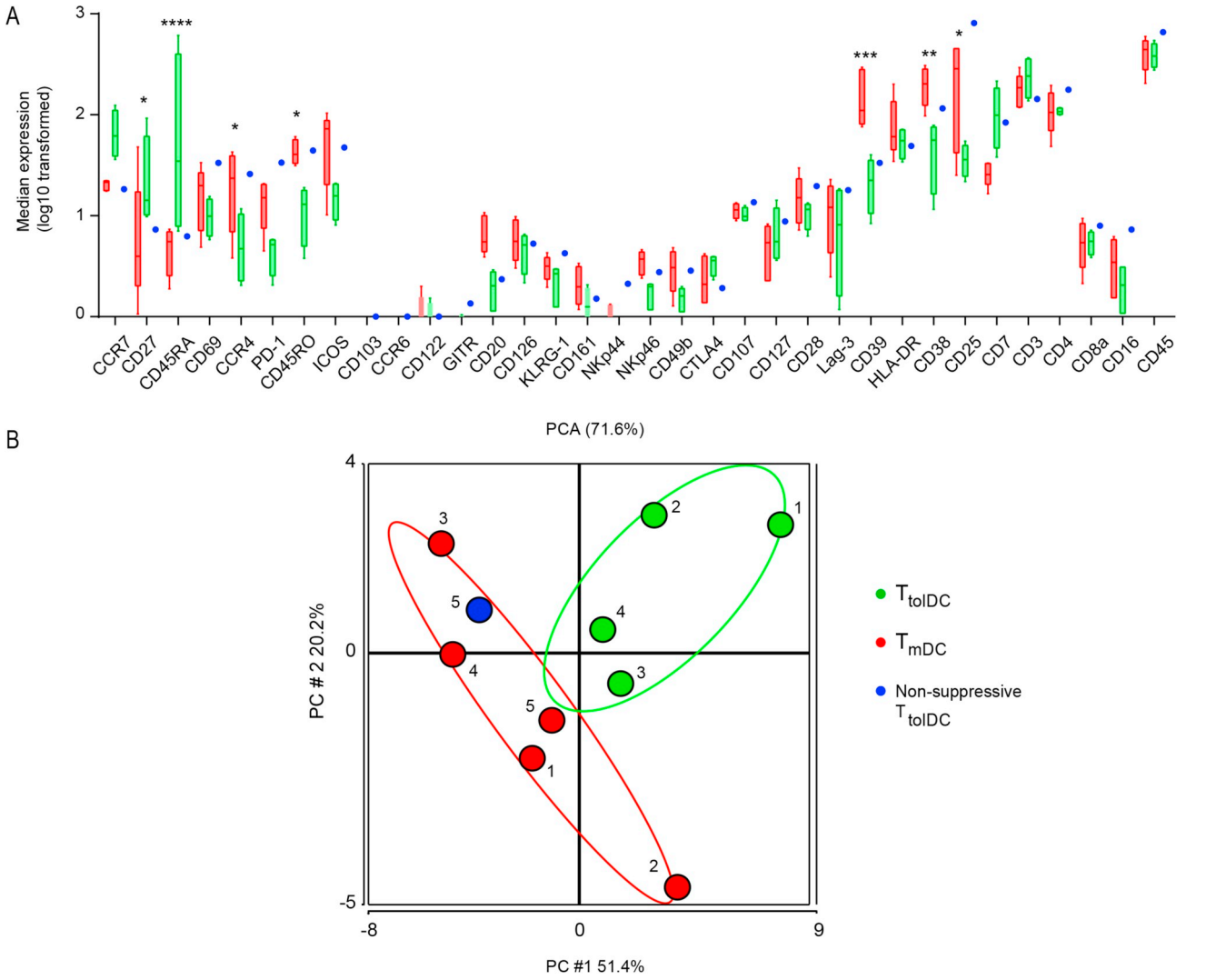

Fig. 2. T_{tolDC} and T_{mDC} lines show distinct phenotypes. T cell lines were stimulated overnight with proinsulin-pulsed mDC and labelled with a CyTOF antibody panel. The green symbols depict suppressive T_{tolDC}, red symbols depict T_{mDC} and blue symbol shows the phenotype of the non-suppressive T_{tolDC} line. **A)** Log10 transformed median expression of T_{tolDC} and T_{mDC}, the whiskers visualise the range minimum to maximum. The lines show different expression of CD27, CD45RA, CCR4, CD45RO, CD39, CD38 and CD25, T_{tolDC} n = 4 and T_{mDC} n = 5 (multiple t-tests; p = 0.049, p < 0.0001, p = 0.049, p = 0.025, p < 0.0001, p = 0.009 and p = 0.01). The non-suppressive T_{tolDC} was not included in the statistical analysis. **B)** Principal Component Analysis of T_{tolDC} and T_{mDC} lines based on the median expression of 35 immune markers. The non-suppressive T_{tolDC} line included in the analyses clusters close to the T_{mDC} lines and separately from the suppressive T_{tolDC} lines. (For interpretation of the references to colour in this figure legend, the reader is referred to the Web version of this article.)

of the 35 tested surface molecules was evaluated, revealing differential expression patterns between T_{tolDC} and T_{mDC} lines (Fig. 2A). T_{tolDC} lines showed higher expression of CD27 and CD45RA than T_{mDC} (multiple t-tests; p = 0.049 and p < 0.0001, respectively). The expression of CCR4, CD45RO, CD39, CD38 and CD25 was lower in T_{tolDC} than in T_{mDC} lines (multiple t-tests; p = 0.049, p = 0.03, p < 0.0001, p = 0.009 and p = 0.01, respectively). The phenotype of the non-suppressive T_{tolDC} line differed from the suppressive T_{tolDC} lines, as well as from T_{mDC} lines. We further performed principal component analysis (PCA) to cluster the generated T cell lines, integrating the median expression patterns of all markers simultaneously (Fig. 2B). The T_{tolDC} and T_{mDC} lines clustered separately, while the non-suppressive T_{tolDC} line

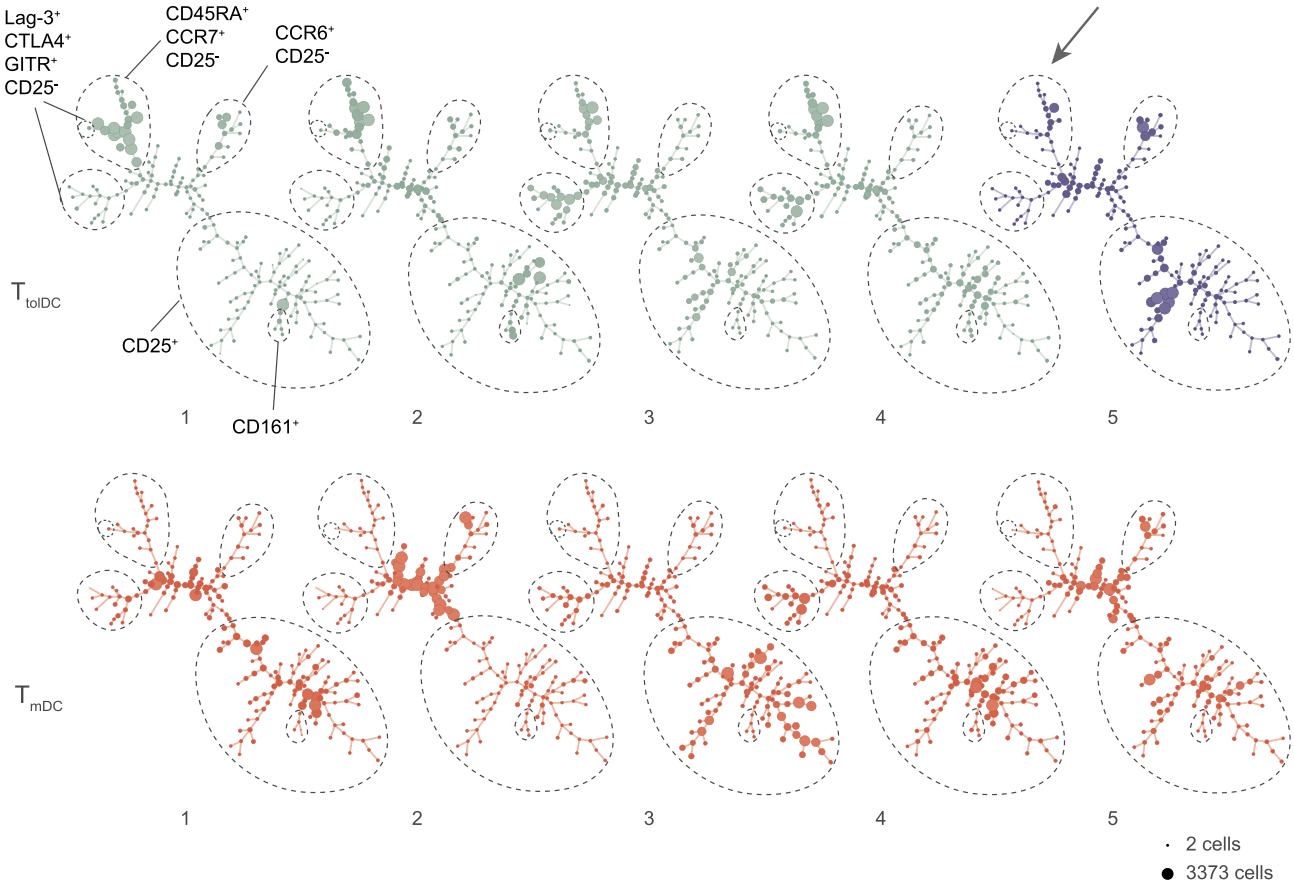

Fig. 3. Multidimensional SPADE analysis of T_{tolDC} and T_{mDC} lines. T_{tolDC} lines (green) show differential cluster distribution in the SPADE analysis from the T_{mDC} lines (red). The non-suppressive T_{tolDC} line (blue) shows different distribution than the suppressive T_{tolDC} lines. Circles depict clusters with designated marker expression as shown in Supplementary Fig. 1. The grey arrow indicates the clusters lacking in the non-suppressive T_{tolDC} line. (For interpretation of the references to colour in this figure legend, the reader is referred to the Web version of this article.)

clustered within the T_{mDC} lines. These results demonstrate differences in surface phenotypes of T cell lines induced by tolDCs versus mDCs.

Next, we analysed the T_{tolDC} and T_{mDC} lines using the SPADE algorithm[30] and visualised these individually to explore the variability between and within T_{tolDC} and T_{mDC} lines. In the SPADE analysis, the multidimensional data set is down sampled and clustered into a two-dimensional tree such that cells with a similar phenotype cluster into a node, where the node branch is based on the differences in the marker expression pattern between clusters (Fig. 3). Overall, T_{tolDC} lines showed different cluster distributions compared to T_{mDC} lines, although variation in cluster size was detectable within the T_{tolDC} or T_{mDC} lines. Moreover, the non-suppressive T_{tolDC} line lacked a group of clusters that were present in the other suppressive T_{tolDC} lines (Fig. 3, grey arrow). To evaluate the phenotype of these clusters, we visualised the marker expressions as a colour overlay (Supplementary Fig. 1). Clusters specific to the suppressive T_{tolDC} lines only were $CD45RA^+CCR7^+CD25^{lo}$. Other three SPADE branches represented distinct clusters of T cells expressing CD25 and CCR6, co-expressing Lag-3, CTLA4 and GITR and were present in both the T_{tolDC} and T_{mDC} lines.

To further dissect the composition of the T_{tolDC} and T_{mDC} lines, a Hierarchical Stochastic Neighbor Embedding (HSNE) analysis was performed. This novel dimensionality reduction technique implemented in the Cytosplore platform[23–25], enabled the analysis of our large data consisting of 1,016,321 cells without having to down sample data by constructing a hierarchy which can be explored stepwise up to the single-cell level. This strategy allows the efficient detection of low frequent cell subsets[25]. A global view of data derived from the T_{tolDC} and T_{mDC} lines is visualised in Fig. 4A. Three main groups were formed using the Gaussian-mean-shift method and each group was further inspected by zooming into the single-cell data level (Fig. 4B). The three main groups were distinguished by the expression of CD45RA, CCR7 and CD25; group A largely consisted of cells expressing CD45RA, CCR7 and low levels of CD25, group B of cells negative for CD45RA and low expression of CCR7 and CD25, and group C of cells lacking CD45RA and CCR7 but expressing high levels of CD25. Further clustering of these groups resulted in seven smaller clusters within group A; seven clusters in group B and six clusters in group C. The phenotypes of the generated clusters were visualised in a heatmap (Fig. 4C) together with the number of cells per cluster originating from the suppressive T_{tolDC} line, non-suppressive T_{tolDC} lines and T_{mDC} lines (Fig. 4C and Supplementary Table 1). The clusters in group A contained T cells with a naïve phenotype (clusters A3-A7) and consisted mainly of suppressive T_{tolDC} cells, matching the SPADE analysis. This group was further characterized by the high expression of CD7 and CD27. Cell clusters A1 and A2 were distinct from the general phenotype of group A, exemplified by the lack of CCR7 expression, demarcating a T_{EMRA} phenotype, of which one cluster (A1) specifically expressed CD161. The clusters in group B displayed an effector memory (EM; $CD45RA^-CCR7^-CD25^{hi}$) phenotype, while group C displayed a central memory (CM; $CD45RA^-CCR7^{lo}CD25^{lo}$) phenotype, consisting of cells derived from both the T_{tolDC} and the T_{mDC} lines. However, T_{mDC} lines contained more EM cells than T_{tolDC} lines, and these co-expressed HLA-DR, CD39, CD38 CD69, ICOS, CD45RO, CD28, PD-1 and CCR4. The clusters with a CM phenotype were also more abundant in T_{mDC} lines, with the exception of two clusters (C4 and C5) co-expressing Lag-3 CTLA4 and GITR, which largely contained T_{tolDC}-originating cells. The signatures of T_{tolDC} and T_{mDC} lines analysed separately in HSNE (Supplementary Fig. 2), confirmed the presence of the specific clusters in T_{tolDC} or T_{mDC} lines.

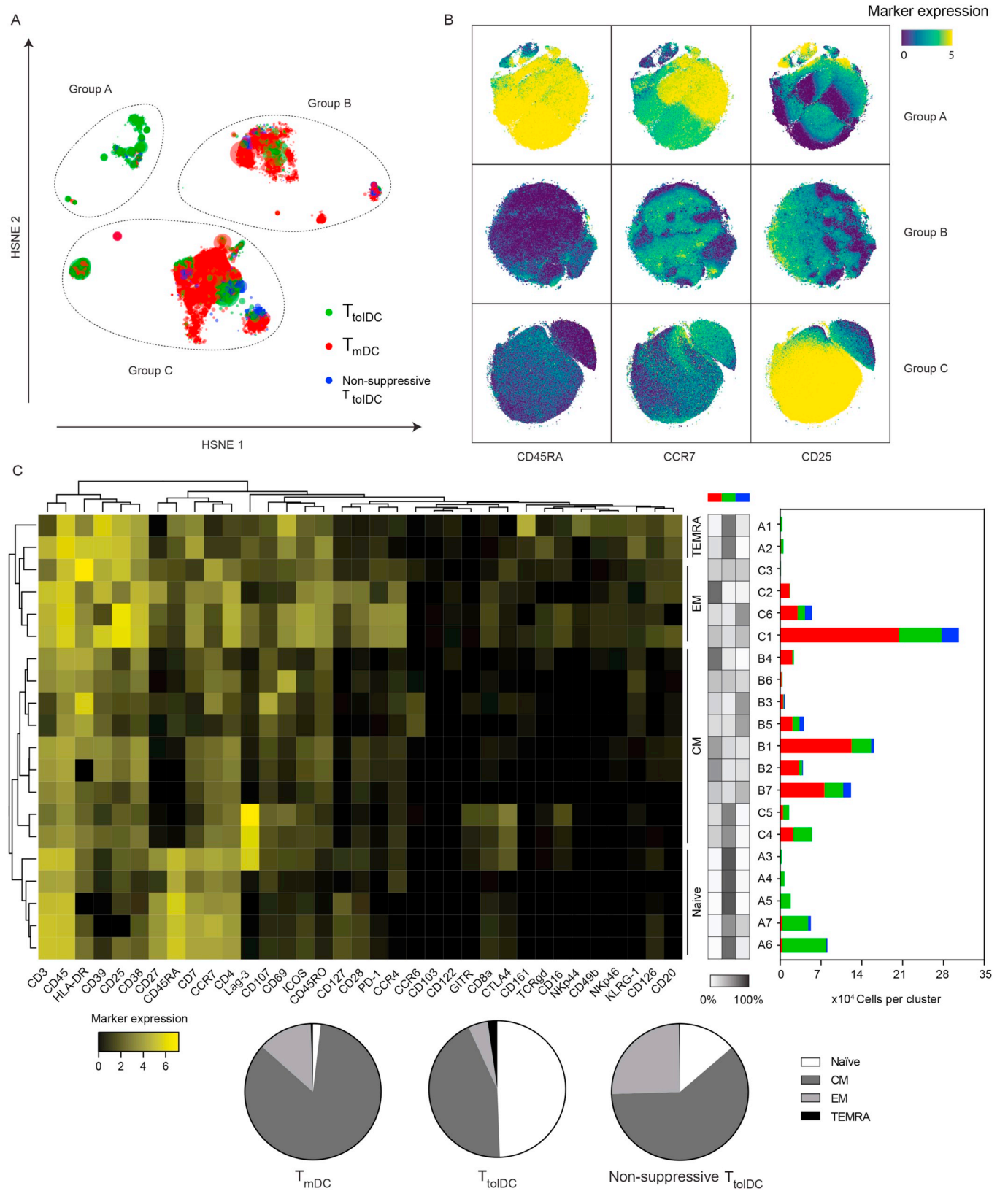

(caption on next page)

In summary, using three independent methods to analyse the phenotype of T_{tolDC} and T_{mDC} cells, we show that T cell lines stimulated with tolDCs acquire substantially different phenotypes than T cells stimulated with mDCs. The abundant presence of $CD45RA^+CCR7^+CD25^{lo}$ naïve T cells marked suppressive T_{tolDC} lines, while cells with CM and EM phenotypes were abundant in both T_{mDC} and T_{tolDC} lines. Two T_{EMRA}-like and two CM subsets were enriched in the suppressive T_{tolDC} lines.

Fig. 4. High dimensional analysis comparing T_{tolDC} and T_{mDC} lines. The CyTOF data of T_{tolDC} and T_{mDC} were analysed together using Hierarchical Stochastic Neighbor Embedding (HSNE). HSNE integrates the information of 35 markers measured on a single cell level in a two-dimensional HSNE map. **A)** Groups A, B and C depict three major landmarks in the HSNE overview level. Green areas depict cells originating from T_{tolDC}, blue areas: cells from the non-suppressive T_{tolDC} line, red areas: cells from T_{mDC} lines. **B)** tSNE plots of landmark groups A, B and C were visualised (at single-cell data level) with respect to expression of CD45RA, CCR7 and CD25. Group A consists mainly of $CD45RA^+$ cells, group B consists of $CD45RA^-$ and $CD25^{lo}$ cells and $CD25^{hi}$ cells were mainly found in group C. **C)** Heatmap of the HSNE. Resulting clusters are visualised as rows in the heatmap. Cluster names refer to the originating group. Heatmap in the middle panel visualises the distribution relative to the number of cells in a cluster. The right histogram shows the abundance of cells within the cluster in absolute numbers, taking into account the origin of cells (green: T_{tolDC}, blue: non-suppressive T_{tolDC} line, red: T_{mDC}). Statistics of the histogram are shown in Supplementary Table 1. The three pie-charts depict the percentage of cells with a naïve, CM, EM or TEMRA phenotype within the T_{mDC}, T_{tolDC} and non-suppressive T_{tolDC} lines. The clusters with a naïve-like phenotype ($CD45RA^+CCR7^+$) were explicitly present in the T_{tolDC} lines. (For interpretation of the references to colour in this figure legend, the reader is referred to the Web version of this article.)

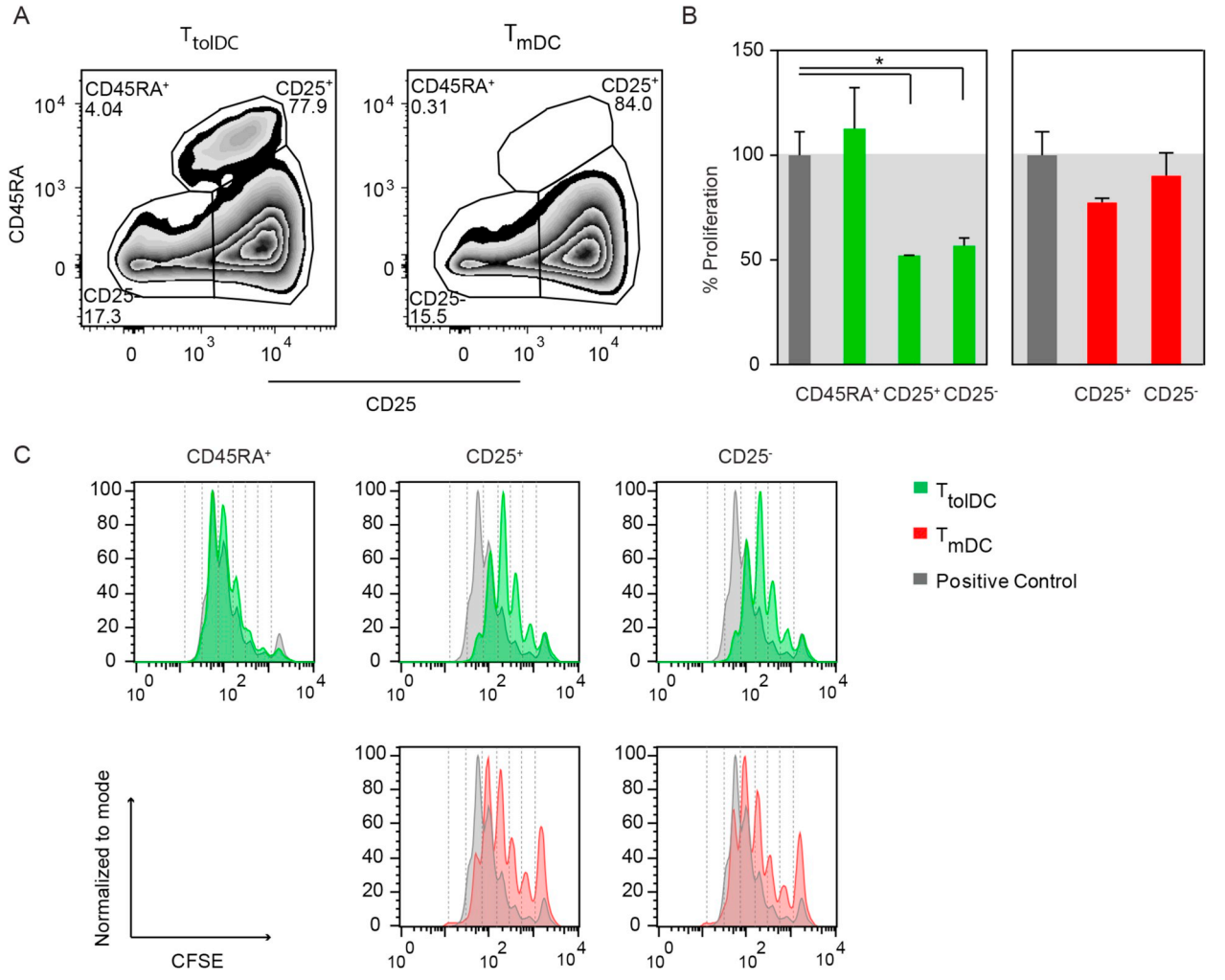

Fig. 5. T_{tolDC} with antigen experienced phenotype suppress naïve T cell proliferation. mDCs pulsed with proinsulin C19A3 were co-cultured T_{tolDC} or T_{mDC} in a 1:10 ratio. Thereafter, T cells were stained and sorted based on CD45RA and CD25 expression. The suppressive capacity of the sorted populations was assessed in a suppression assay. **A)** Gating strategy of the cell sorting. **B and C)** Graphs and histograms depict proliferation of the CFSE-labelled allogeneic responder T cells in the presence of sorted T_{tolDC} (green) or sorted T_{mDC} (red) subsets relative to the responder proliferation alone (grey). Sorted memory-like $CD25^{hi}$ and $CD25^{lo}$, but not naïve-like $CD45RA^+$ cells from T_{tolDC} lines suppressed naïve T cell proliferation (one-way ANOVA $p = 0.03$ and $p = 0.04$). In contrast, sorted T_{mDC} were not suppressive, irrespective of CD25 expression. Graphs depict representative of 2 independent experiments using T cell lines from different donors with similar results. (For interpretation of the references to colour in this figure legend, the reader is referred to the Web version of this article.)

3.3. Suppressive capacity of T_{tolDC} and T_{mDC} subpopulations

To evaluate which of the three groups of cells in the T_{tolDC} lines defined by the multidimensional phenotypic analyses contains T cells with suppressive capacity, cells from T_{tolDC} and T_{mDC} lines were sorted based on the expression of CD45RA and CD25 and tested in a suppression assay (Fig. 5). The $CD45RA^+$ T cells (representing group A) were only present in the suppressive T_{tolDC} line but lacked suppressive capacity. In contrast, both $CD45RA^-CD25^{hi}$ and $CD45RA^-CD25^{lo}$ T cells (representing group C and B, respectively) sorted from T_{tolDC} lines showed suppressive capacity (Fig. 5B and C; one-way ANOVA $p = 0.03$ and $p = 0.04$), whereas $CD45RA^-CD25^{hi}$ and $CD45RA^-CD25^{lo}$ T cells derived from T_{mDC} did not suppress allogeneic $CD4^+$ T cell proliferation (Fig. 5B and C).

Next, we evaluated whether T_{tolDC} can inhibit target-cell killing by autoreactive $CD8^+$ T cells. For this, clonal preproinsulin (PPI)-specific $CD8^+$ T cells were incubated with PPI-peptide pulsed target cells in the presence of total or sorted T_{tolDC} populations. From the sorted T_{tolDC}

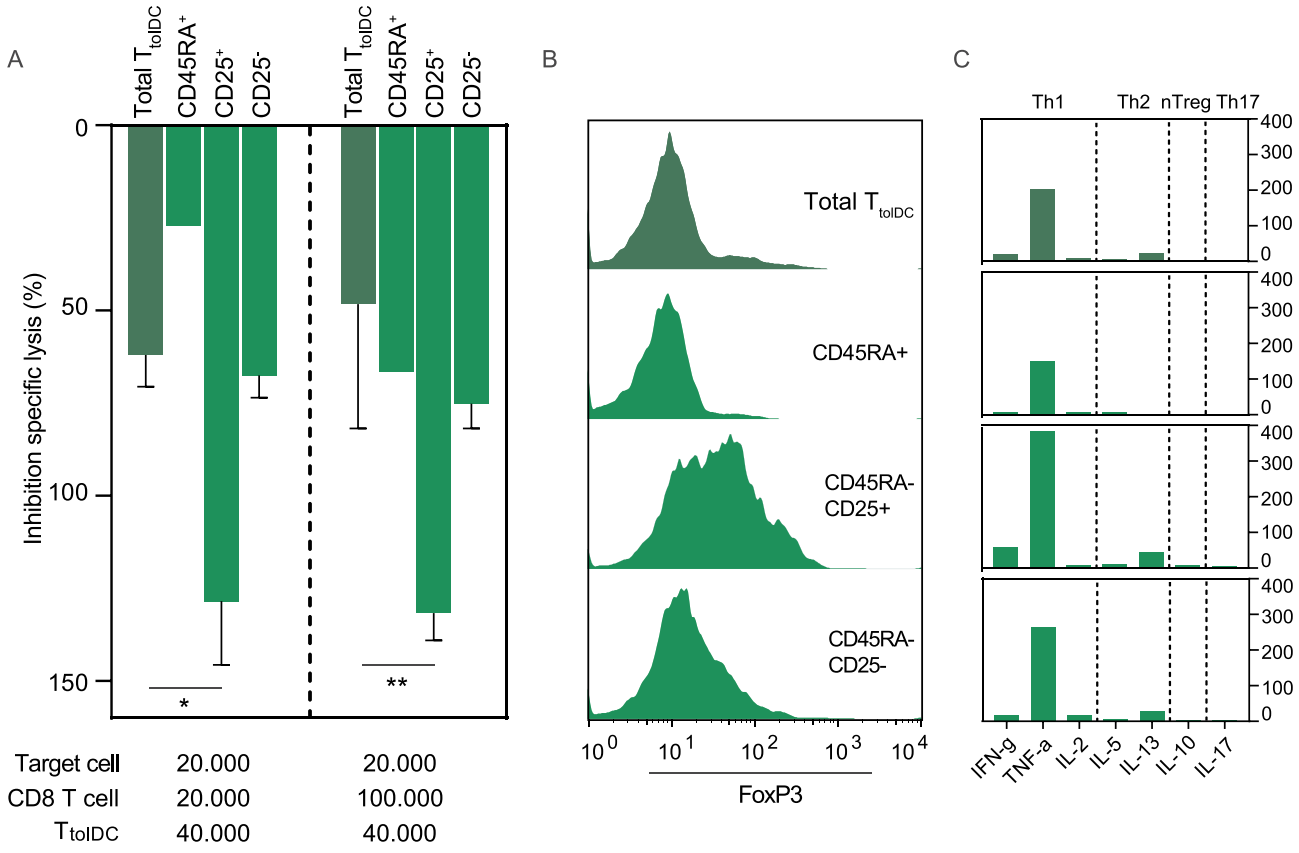

Fig. 6. Memory-like T_{tolDC} expressing $CD25^{hi}$ protect target cells from CD8-induced killing. T_{tolDC} were stimulated overnight with proinsulin pulsed mDC. Thereafter, T_{tolDC} cells were sorted into 3 groups based on the expression of CD45RA and CD25 ($CD45RA^+$, $CD45RA^-CD25^{lo}$ and $CD45RA^-CD25^{hi}$). **A)** The ability to inhibit $CD8^+$ T cell-induced killing was tested using PPI-specific $CD8^+$ T cell clone as effector and B cells loaded with PPI-peptide as target. Total T_{tolDC} or sorted subsets were incubated with CFSE-labelled target cells in a 2:1 ratio overnight. PPI-specific $CD8^+$ T cells were added for 4 h, after which target cell counts were measured and % specific cell lysis was calculated. Specific lysis in the condition without T_{tolDC} were approximately 10% and 20% respectively, and were set to the maximum (0% inhibition). Data are shown as mean % inhibition ± SD. From the T_{tolDC} subpopulations, $CD45RA^-CD25^{hi}$ T_{tolDC} shows significant inhibition of $CD8^+$ T cell induced killing compared to the unsorted T_{tolDC} (two-way ANOVA; $p = 0.017$ and $p = 0.0058$). **B)** Intracellular Foxp3 expression of T_{tolDC} line and the sorted T cell populations after overnight stimulation with proinsulin peptide-pulsed mDC. **C)** Cytokine production by total and sorted T_{tolDC} after overnight stimulation with proinsulin peptide-pulsed mDC.

subpopulations, memory $CD45RA^-CD25^{hi}$ T_{tolDC} were most capable of inhibiting $CD8^+$ T cell-induced killing (Fig. 6A; two-way ANOVA $p = 0.017$ and $p = 0.0058$), while inhibition by $CD45RA^+$ and $CD45RA^-CD25^{lo}$ T_{tolDC} was insignificant compared to the total T_{tolDC}. The inhibiting capacity of the unsorted T_{tolDC} line was likely limited, since the inhibiting $CD45RA^-CD25^{hi}$ subset represented a small proportion of the total T_{tolDC} (approximately 7%).

To further characterize the T_{tolDC} subpopulations, activation-induced Foxp3 expression was determined upon stimulation with proinsulin pulsed mDC. $CD45RA^-CD25^{hi}$ and $CD45RA^-CD25^{lo}$ T_{tolDC} showed high or intermediate expression of intracellular Foxp3, respectively, while $CD45RA^+$ T_{tolDC} did not express Foxp3. Lastly, cytokines were measured in the supernatant of T_{tolDC} subpopulations after re-challenge with proinsulin-pulsed mDC. Minor amounts of cytokines were detected in the supernatant of total T_{tolDC} (Fig. 6C), corresponding with the data from unsorted T_{tolDC} lines (Fig. 1C). The majority of cytokines produced by T_{tolDC} was derived from the $CD45RA^-CD25^{hi}$ and $CD45RA^-CD25^{lo}$ populations, while cytokine production by $CD45RA^+$ T_{tolDC} was nearly undetectable.

From this, we conclude that $CD45RA^+$ T_{tolDC} are non-activated, Foxp3-negative T cells, while T_{tolDC} with $CD45RA^-CD25^{hi}$ and $CD45RA^-CD25^{lo}$ phenotypes contain activated T cells with regulating capacity.

4. Discussion

In this study, we extensively characterized the surface phenotypes and function of T cells stimulated with proinsulin peptide-pulsed tolDCs. Non-suppressive T cells were generated by tolDCs with an aberrant phenotype, underscoring the critical importance of CD52 and CD86 expression as quality control markers for tolDCs' ability to induce suppressive Tregs[29]. Combining high-dimensional phenotyping with functional assays, we discovered that the presence of unresponsive, Foxp3 negative T cells holding a naïve-like phenotype ($CD45RA^+CCR7^+$) characterized suppressive T cell cultures induced by tolDCs. The functional suppressive T cells in tolDC-stimulated cultures lost CD45RA and obtained either $CCR7^+CD25^{lo}$ central memory or $CCR7^-CD25^{hi}$ effector memory phenotypes. Both subsets were capable of suppressing allogeneic $CD4^+$ T cell proliferation, while the inhibition of $CD8^+$ T cell killing was unique for effector memory $CD45RA^-CD25^{hi}$ T_{tolDC}. Contrary to IL-10-induced Tr1 [17,18], suppressive T_{tolDC} did not produce anti-inflammatory cytokines, supporting our earlier observation on strongly suppressive Treg clones [22], while blocking of IL-10 and TGF-b did not affect the suppressive activity of tolDC-induced Tregs [8].

We propose that the naïve T cell population in T_{tolDC} lines reflects their arrest in activation and differentiation secondary to the concomitant induction of regulatory T cells. RNAseq analyses revealed several genes upregulated in tolDCs that are associated with inhibition

of cell activation[29]. Indeed, yields of T_{tolDC} after two weeks of culture rarely exceeded the number of plated naïve T cells at the start of the culture. In addition, T cell cultures stimulated by tolDCs never formed cell-clusters and retained the round morphology of inactive T cells (data not shown), possibly reflecting specific gene expression modifying the tolDC capacity to interact with cells and extracellular matrix[29]. Which inhibitory molecules on tolDC or soluble mediators determine the lack of close contact with T cells including the underlying mechanisms remain to be investigated.

The mechanisms by which tolDC-induced Tregs modulate immune responses *in vivo* can be diverse. Islet infiltrating lymphocytes rarely contain Tregs in human T1D [31,32]. Instead, Tregs could protect beta cells (lacking HLA class II) indirectly by modifying antigen specific cells (APC) presenting proinsulin peptide in pancreas draining lymph nodes which in turn inhibit effector T cells and protect pancreatic beta cells [8]. Tregs may also induce bystander suppression of neighboring T cells by scavenging for essential cytokines and nutrients. Indeed, effector memory T_{tolDC} in this study showed low IL-2 content in the supernatant and inhibited islet autoreactive $CD8^+$ T cells, while expressing more Foxp3 than central memory T_{tolDC}. This difference could be explained by high expression of IL-2Rα (CD25), enabling this subset to capture and deprive other cells from IL-2, a mechanism proven essential to limit $CD8^+$ T cell activation but not to control $CD4^+$ T cell responses [33]. In addition, the signaling by the captured IL-2 could support higher Foxp3 expression in this subset[34].

Using mass cytometry based analysis, the memory T_{tolDC} populations were further subdivided into clusters characterized by expression of previously described Treg markers such as HLA-DR [35], CD39 [36], Lag-3 [37], CTLA4 [38], ICOS [39], CCR4 [40] and CD161 [41,42]. T_{tolDC} with an effector memory phenotype co-expressed the markers CD28, CD38, CD39, CCR4, HLA-DR, ICOS and PD-1. In our analysis, we found a distinct population enriched in the T_{tolDC} lines co-expressing Lag-3, CTLA4 and GITR within the central memory and naïve phenotype. In addition, a small population characterized by CD161 was found within the T_{EMRA} phenotype suggesting that T cells with T_{EMRA} phenotype contain adaptive Tregs. This concurs with reports suggesting that T_{EMRA} are not merely unresponsive, exhausted cells[43]. In view of their low frequency however, it is unlikely that only $CD161^+$ cells contribute to the suppressive activity of the $CD25^{hi}$ subset. Based on our findings here and our previous work[8], we presume that different T cell subsets such as $CD161^+$ and Lag-3^+ T cells contribute to the suppressive capacity of tolDC-induced Tregs.

The complexity and diversity of circulating nTregs has been described using mass cytometry and resembles the phenotypical signature that we report here on the tolDC-stimulated T cell lines, as well as those we reported previously [21,22]. nTregs, too, can be subdivided into several populations expressing CD45RO, CCR4, HLA-DR, ICOS, CD38, CD39 and a distinct $CD161^+$ population. Although this would suggest that induced antigen-specific Tregs look similar to $Foxp3^+$ nTregs, our studies show that most of these markers can also be present on activated non-suppressive T cells. Furthermore, we demonstrated that tolDCs also induce antigen-specific Tregs with $CD25^{lo}$ and $Foxp3^{dim}$ phenotype. Additional markers are therefore needed to identify induced suppressive cells in peripheral blood following immune modifying therapies. Subpopulations with unique suppressive qualities were identified, prompting follow-up analyses using an extended list of suppression-associated surface and intracellular molecules. The regulatory phenotypes described here may provide viable biomarkers of immune regulation in the clinic, enabling detection of induced Tregs after tolDC administration *in vivo*.

5. Conclusions

In summary, multiparameter analysis revealed phenotypical signatures of tolDC-stimulated T cells and showed that tolDC-induced Tregs obtain differential phenotypes, which corresponds to earlier findings of Treg diversity. We additionally demonstrate that partial tolerogenic modulation of DCs reflects in an atypical tolDC phenotype and reduced the Treg-inducing capacity. Suppressive T cells induced by tolDCs acquire different memory phenotypes, including cells expressing Lag-3, CD161 and ICOS. These markers, however, are also expressed by non-suppressive T cells. TolDC-induced T cell lines also retain or fix naïve-like T cells in a non-activated and non-suppressive state. This, however, mirrors the induction of suppressive activity. Our combined findings *in vitro* provide a basis for monitoring and optimization of the clinical use of tolDC therapies.

Authorship contributions

JSS, SL, KV, AJ and TN carried out the experiments. JSS, SL and TN performed the data analysis with support of VvU. VvU, BPFL and TH developed software for the data analysis and contributed to the study design. JSS, SL, TN, JJZ and BOR wrote the manuscript. BOR conceived the project and secured funding for this study.

Funding

This work was supported by the Wanek Family Project for Type 1 Diabetes, the Dutch Diabetes Research Foundation (grant number 31187) and the Dutch Arthritis Foundation (grant number 30514).

Acknowledgements

We thank Guillaume Beyrend for help with the data analysis and programming in R.

Appendix A. Supplementary data

Supplementary data to this article can be found online at https://doi.org/10.1016/j.jaut.2019.102361.

References

[1] S.E. Gitelman, J.A. Bluestone, Regulatory T cell therapy for type 1 diabetes: may the force be with you, J. Autoimmun. 71 (2016) 78–87.
[2] N. Marek-Trzonkowska, M. Mysliwiec, A. Dobyszuk, M. Grabowska, I. Techmanska, J. Juscinska, et al., Administration of CD4+CD25highCD127- regulatory T cells preserves beta-cell function in type 1 diabetes in children, Diabetes Care 35 (2012) 1817–1820.
[3] A.L. Putnam, T.M. Brusko, M.R. Lee, W. Liu, G.L. Szot, T. Ghosh, et al., Expansion of human regulatory T-cells from patients with type 1 diabetes, Diabetes 58 (2009) 652–662.
[4] J.A. Todd, M. Evangelou, A.J. Cutler, M.L. Pekalski, N.M. Walker, H.E. Stevens, et al., Regulatory T cell responses in participants with type 1 diabetes after a single dose of interleukin-2: a non-randomised, open label, adaptive dose-finding trial, PLoS Med. 13 (2016) e1002139.
[5] M. Alhadj Ali, Y.F. Liu, S. Arif, D. Tatovic, H. Shariff, V.B. Gibson, et al., Metabolic and immune effects of immunotherapy with proinsulin peptide in human new-onset type 1 diabetes, Sci. Transl. Med. 9 (2017).
[6] G.B. Ferreira, F.S. Kleijwegt, E. Waelkens, K. Lage, T. Nikolic, D.A. Hansen, et al., Differential protein pathways in 1,25-dihydroxyvitamin d(3) and dexamethasone modulated tolerogenic human dendritic cells, J. Proteome Res. 11 (2012) 941–971.
[7] F.S. Kleijwegt, B.O. Roep, Infectious tolerance as candidate therapy for type 1 diabetes: transfer of immunoregulatory properties from human regulatory T cells to other T cells and proinflammatory dendritic cells, Crit. Rev. Immunol. 33 (2013) 415–434.
[8] F.S. Kleijwegt, S. Laban, G. Duinkerken, A.M. Joosten, B.P. Koeleman, T. Nikolic, et al., Transfer of regulatory properties from tolerogenic to proinflammatory dendritic cells via induced autoreactive regulatory T cells, J. Immunol. 187 (2011) 6357–6364.
[9] W.W. Unger, S. Laban, F.S. Kleijwegt, A.R. van der Slik, B.O. Roep, Induction of Treg by monocyte-derived DC modulated by vitamin D3 or dexamethasone: differential role for PD-L1, Eur. J. Immunol. 39 (2009) 3147–3159.
[10] F.S. Kleijwegt, D.T. Jansen, J. Teeler, A.M. Joosten, S. Laban, T. Nikolic, et al., Tolerogenic dendritic cells impede priming of naive CD8(+) T cells and deplete memory CD8(+) T cells, Eur. J. Immunol. 43 (2013) 85–92.
[11] J.S. Suwandi, T. Nikolic, B.O. Roep, Translating mechanism of regulatory action of tolerogenic dendritic cells to monitoring endpoints in clinical trials, Front. Immunol. 8 (2017) 1598.
[12] B.O. Roep, F.S. Kleijwegt, A.G. van Halteren, V. Bonato, U. Boggi, F. Vendrame,

et al., Islet inflammation and CXCL10 in recent-onset type 1 diabetes, Clin. Exp. Immunol. 159 (2010) 338–343.
[13] V.B. Gibson, T. Nikolic, V.Q. Pearce, J. Demengeot, B.O. Roep, M. Peakman, Proinsulin multi-peptide immunotherapy induces antigen-specific regulatory T cells and limits autoimmunity in a humanized model, Clin. Exp. Immunol. 182 (2015) 251–260.
[14] S. Hori, T. Nomura, S. Sakaguchi, Control of regulatory T cell development by the transcription factor Foxp3, Science 299 (2003) 1057–1061.
[15] C.L. Bennett, J. Christie, F. Ramsdell, M.E. Brunkow, P.J. Ferguson, L. Whitesell, et al., The immune dysregulation, polyendocrinopathy, enteropathy, X-linked syndrome (IPEX) is caused by mutations of FOXP3, Nat. Genet. 27 (2001) 20–21.
[16] H.J.J. van der Vliet, E.E. Nieuwenhuis, IPEX as a result of Mutations in FOXP3, Clin. Dev. Immunol. 2007 (2007), https://doi.org/10.1155/2007/89017.
[17] M.G. Roncarolo, R. Bacchetta, C. Bordignon, S. Narula, M.K. Levings, Type 1 T regulatory cells, Immunol. Rev. 182 (2001) 68–79.
[18] M.G. Roncarolo, S. Gregori, M. Battaglia, R. Bacchetta, K. Fleischhauer, M.K. Levings, Interleukin-10-secreting type 1 regulatory T cells in rodents and humans, Immunol. Rev. 212 (2006) 28–50.
[19] S.E. Allan, S.Q. Crome, N.K. Crellin, L. Passerini, T.S. Steiner, R. Bacchetta, et al., Activation-induced FOXP3 in human T effector cells does not suppress proliferation or cytokine production, Int. Immunol. 19 (2007) 345–354.
[20] M. Kmieciak, M. Gowda, L. Graham, K. Godder, H.D. Bear, F.M. Marincola, et al., Human T cells express CD25 and Foxp3 upon activation and exhibit effector/memory phenotypes without any regulatory/suppressor function, J. Transl. Med. 7 (2009).
[21] G.M. Mason, K. Lowe, R. Melchiotti, R. Ellis, E. de Rinaldis, M. Peakman, et al., Phenotypic complexity of the human regulatory T cell compartment revealed by mass cytometry, J. Immunol. 195 (2015) 2030–2037.
[22] D.X. Beringer, F.S. Kleijwegt, F. Wiede, A.R. van der Slik, K.L. Loh, J. Petersen, et al., T cell receptor reversed polarity recognition of a self-antigen major histocompatibility complex, Nat. Immunol. 16 (2015) 1153–1161.
[23] T. Hollt, N. Pezzotti, V. van Unen, F. Koning, E. Eisemann, B. Lelieveldt, et al., Cytosplore: interactive immune cell phenotyping for large single-cell datasets, Comput. Graph. Forum 35 (2016) 171–180.
[24] N. Pezzotti, T. Hollt, B. Lelieveldt, E. Eisemann, A. Vilanova, Hierarchical stochastic neighbor embedding, Comput. Graph. Forum 35 (2016) 21–30.
[25] V. van Unen, T. Hollt, N. Pezzotti, N. Li, M.J.T. Reinders, E. Eisemann, et al., Visual analysis of mass cytometry data by hierarchical stochastic neighbour embedding reveals rare cell types, Nat. Commun. 8 (2017).
[26] S. Laban, J.S. Suwandi, V. van Unen, J. Pool, J. Wesselius, T. Hollt, et al., Heterogeneity of circulating CD8 T-cells specific to islet, neo-antigen and virus in patients with type 1 diabetes mellitus, PLoS One 13 (2018) e0200818.
[27] N. Kotecha, P.O. Krutzik, J.M. Irish, Web-based analysis and publication of flow cytometry experiments, Curr Protoc Cytom 53 (1) (2010) 10.17.1–10.17.24, https://doi.org/10.1002/0471142956.cy1017s53.
[28] F.S. Kleijwegt, S. Laban, G. Duinkerken, A.M. Joosten, A. Zaldumbide, T. Nikolic, et al., Critical role for TNF in the induction of human antigen-specific regulatory T cells by tolerogenic dendritic cells, J. Immunol. 185 (2010) 1412–1418.
[29] T. Nikolic, N.J.C. Woittiez, A. van der Slik, S. Laban, A. Joosten, C. Gysemans, et al., Differential transcriptome of tolerogenic versus inflammatory dendritic cells points to modulated T1D genetic risk and enriched immune regulation, Genes Immun. 18 (2017) 176–183.
[30] M.J. Zaki, SPADE: an efficient algorithm for mining frequent sequences, Mach. Learn. 42 (2001) 31–60.
[31] C.M. Hull, M. Peakman, T.I.M. Tree, Regulatory T cell dysfunction in type 1 diabetes: what's broken and how can we fix it? Diabetologia 60 (2017) 1839–1850.
[32] A. Willcox, S.J. Richardson, A.J. Bone, A.K. Foulis, N.G. Morgan, Analysis of islet inflammation in human type 1 diabetes, Clin. Exp. Immunol. 155 (2009) 173–181.
[33] T. Chinen, A.K. Kannan, A.G. Levine, X. Fan, U. Klein, Y. Zheng, et al., An essential role for the IL-2 receptor in Treg cell function, Nat. Immunol. 17 (2016) 1322–1333.
[34] E. Zorn, E.A. Nelson, M. Mohseni, F. Porcheray, H. Kim, D. Litsa, et al., IL-2 regulates FOXP3 expression in human CD4+CD25+ regulatory T cells through a STAT-dependent mechanism and induces the expansion of these cells in vivo, Blood 108 (2006) 1571–1579.
[35] C. Baecher-Allan, E. Wolf, D.A. Hafler, MHC class II expression identifies functionally distinct human regulatory T cells, J. Immunol. 176 (2006) 4622–4631.
[36] K.M. Dwyer, D. Hanidziar, P. Putheti, P.A. Hill, S. Pommey, J.L. McRae, et al., Expression of CD39 by human peripheral blood CD4+ CD25+ T cells denotes a regulatory memory phenotype, Am. J. Transplant. 10 (2010) 2410–2420.
[37] C.T. Huang, C.J. Workman, D. Flies, X. Pan, A.L. Marson, G. Zhou, et al., Role of LAG-3 in regulatory T cells, Immunity 21 (2004) 503–513.
[38] L.S. Walker, Treg and CTLA-4: two intertwining pathways to immune tolerance, J. Autoimmun. 45 (2013) 49–57.
[39] T. Ito, S. Hanabuchi, Y.H. Wang, W.R. Park, K. Arima, L. Bover, et al., Two functional subsets of FOXP3+ regulatory T cells in human thymus and periphery, Immunity 28 (2008) 870–880.
[40] D. Sugiyama, H. Nishikawa, Y. Maeda, M. Nishioka, A. Tanemura, I. Katayama, et al., Anti-CCR4 mAb selectively depletes effector-type FoxP3+CD4+ regulatory T cells, evoking antitumor immune responses in humans, Proc. Natl. Acad. Sci. U. S. A. 110 (2013) 17945–17950.
[41] B. Afzali, P.J. Mitchell, F.C. Edozie, G.A. Povoleri, S.E. Dowson, L. Demandt, et al., CD161 expression characterizes a subpopulation of human regulatory T cells that produces IL-17 in a STAT3-dependent manner, Eur. J. Immunol. 43 (2013) 2043–2054.
[42] A.M. Pesenacker, D. Bending, S. Ursu, Q. Wu, K. Nistala, L.R. Wedderburn, CD161 defines the subset of FoxP3+ T cells capable of producing proinflammatory cytokines, Blood 121 (2013) 2647–2658.
[43] J.M. Faint, N.E. Annels, S.J. Curnow, P. Shields, D. Pilling, A.D. Hislop, et al., Memory T cells constitute a subset of the human CD8+CD45RA+ pool with distinct phenotypic and migratory characteristics, J. Immunol. 167 (2001) 212–220.